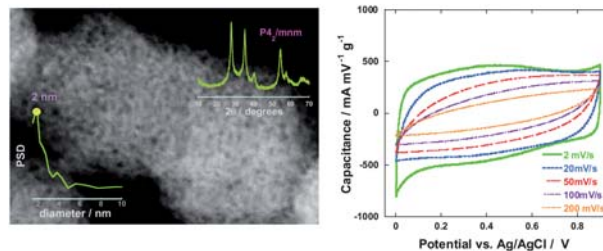


**Direct synthesis of electroactive mesoporous hydrous crystalline RuO<sub>2</sub> templated by a cationic surfactant**

Si Hyoung Oh and Linda F. Nazar\*

A direct surfactant templating and crystallization route was developed to synthesize a quasi-ordered crystalline mesoporous RuO<sub>2</sub>·0.4H<sub>2</sub>O with a high surface area up to 250 m<sup>2</sup> g<sup>-1</sup> which exhibits high capacitance of 410 F g<sup>-1</sup> and good rate capability.



Please check this proof carefully. **Our staff will not read it in detail after you have returned it.**

Translation errors between word-processor files and typesetting systems can occur so the whole proof needs to be read. Please pay particular attention to: tabulated material; equations; numerical data; figures and graphics; and references. If you have not already indicated the corresponding author(s) please mark their name(s) with an asterisk. Please e-mail a list of corrections or the PDF with electronic notes attached – do not change the text within the PDF file or send a revised manuscript.

**Please bear in mind that minor layout improvements, e.g. in line breaking, table widths and graphic placement, are routinely applied to the final version.**

We will publish articles on the web as soon as possible after receiving your corrections; no late corrections will be made.

Please return your **final** corrections, where possible within **48 hours** of receipt by e-mail to: [materials@rsc.org](mailto:materials@rsc.org)

Reprints—Electronic (PDF) reprints will be provided free of charge to the corresponding author. Enquiries about purchasing paper reprints should be addressed via: <http://www.rsc.org/Publishing/ReSource/PaperReprints/>. Costs for reprints are below:

**Reprint costs**

No of pages	Cost for 50 copies	Cost for each additional 50 copies
2–4	£190	£120
5–8	£315	£230
9–20	£630	£500
21–40	£1155	£915
>40	£1785	£1525

*Cost for including cover of journal issue:*  
£55 per 50 copies

# Direct synthesis of electroactive mesoporous hydrous crystalline RuO<sub>2</sub> templated by a cationic surfactant

Si Hyoung Oh and Linda F. Nazar\*

Received 21st December 2009, Accepted 21st January 2010

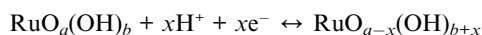
First published as an Advance Article on the web

DOI: 10.1039/b926734d

We describe a direct low-temperature, liquid crystal surfactant templating and crystallization route to form quasi-ordered crystalline mesoporous RuO<sub>2</sub> · 0.4H<sub>2</sub>O. Our method constitutes a direct approach to the crystalline oxide, which is constructed of nanosized metal oxide building blocks (a few nm in size) that are assembled to form thin walls. This leads to high surface area up to 250 m<sup>2</sup> g<sup>-1</sup>. In our approach, cationic surfactants (hexadecyl-trimethylammonium chloride, C<sub>16</sub>TMA<sup>+</sup>Cl<sup>-</sup>) serve as pore-directing agents which can participate in an indirect S<sup>+</sup>X<sup>-</sup>I<sup>+</sup> interaction mediated by the chloride ion, to coordinate a cationic ruthenium nitrosyl precursor. Gentle decomposition of the initially formed mesostructured metal cation–surfactant composite leads to crystallization of the wall structure. The promising electrochemical properties of porous RuO<sub>2</sub> · xH<sub>2</sub>O result from a more highly ordered structure and almost tripled surface area (190 m<sup>2</sup> g<sup>-1</sup>) compared to that obtained from the nanocasting method. Crystalline mesoporous RuO<sub>2</sub> · 0.4H<sub>2</sub>O exhibits high capacitance of 410 F g<sup>-1</sup> and good rate capability, whereas the amorphous mesoporous RuO<sub>2</sub> · 1.3H<sub>2</sub>O displays capacitance over 700 F g<sup>-1</sup>.

## Introduction

The synthesis of hexagonally ordered mesoporous silica MCM-41<sup>1,2</sup> over a decade ago introduced a revolutionary new method for preparing various 2-D and 3-D periodic materials. Extension to mesoporous transition metal oxides (MTMOs) still remains a considerable challenge for redox-active metals, however. MTMOs are of substantial interest because of their characteristic functional properties and ability to adopt a wide range of valence states. They have immense potential for control of catalytic and photocatalytic reactions;<sup>3,4</sup> separation or storage of ions/electrons/molecules for energy conversion and storage;<sup>5,6</sup> as redox active surfaces for electrochemical reactions;<sup>7,8</sup> and as chemical sensors.<sup>9</sup> A relatively crystalline wall structure is often highly desirable for these applications. A good example is metallic RuO<sub>2</sub> which has many functional properties that are highly dependent on its crystalline nature, surface area and accessibility of the redox centres. This metallic oxide is reported to be an excellent catalyst for CO oxidation,<sup>10</sup> an interesting lithium-ion battery electrode material,<sup>11,12</sup> and is especially regarded as being amongst the most promising electrode materials for supercapacitor applications in the last decade.<sup>13–15</sup> Its high fundamental energy storage capability derives from pseudocapacitance arising from the surface redox reactions of RuO<sub>2</sub>. They involve the simultaneous injections of protons and electrons:



The capacitive storage and rate capability are greatly enhanced when the electronic and protonic transports are optimized in

concert. Key to this is establishing a continuous nanocrystalline network that maintains low-defect metallic conduction pathways, but also possesses sufficient surface area and hydration for proton access. While it is possible to synthesize high surface area RuO<sub>2</sub> that exhibits textural porosity by virtue of tiny crystallite dimensions, tailoring a framework to possess long-range structural micro- and mesoporosity has proved more demanding. Thus the direct formation of highly porous hydrated crystalline RuO<sub>2</sub> without collapse of the wall structure and subsequent loss of integrity remains a major challenge. This is common to most porous transition metal oxides. Their tendency to disintegrate during template removal and/or annealing derives from the thermodynamic forces that drive the formation of a dense crystalline structure favored by TMO's.

Previous research on MTMOs based on high or fixed oxidation state metal oxides shows they can be prepared by approaches that can generally be divided into two classes. The soft or direct template route is based on a one-pot synthesis of metal oxides using surfactants as structure-directing reagents, as in the case of silica. Although the resulting metal oxides often exhibit fragile amorphous frameworks that undergo the above-mentioned collapse on heating, several fixed oxidation state metal oxides such as zirconia, titania, alumina, niobia and tantalum have been recently prepared by this method. The more successful nanocasting route involves a hard-templating approach that relies on an inverse template method. The scaffolds (e.g., mesoporous silica or carbon and polymer or silica lattices) are used to nucleate the metal oxide structure, and are then removed *via* etching or calcination. The nanocasting route is cumbersome, though the templates must be removed by aqueous leaching in hot NaOH or HF solution, a process that can result in structural degradation. Nonetheless, many MTMOs have been synthesized by this method, including Fe<sub>2</sub>O<sub>3</sub>,<sup>16</sup> β-MnO<sub>2</sub>,<sup>17</sup> Co<sub>3</sub>O<sub>4</sub>,<sup>18</sup> NiO,<sup>19</sup> and CuO.<sup>20</sup> Mesoporous RuO<sub>2</sub> has also been

Department of Chemistry, University of Waterloo, Waterloo, ON, Canada.  
E-mail: lnazar@uwaterloo.ca

1 prepared *via* nanocasting, but the material was very poorly  
ordered and displayed low-intermediate surface area.<sup>10</sup> A clever  
approach to obtain crystalline mesoporous metal oxides uses the  
5 high-temperature crystallization of amorphous metal oxides in  
the presence of glassy phases such as silica,<sup>21</sup> phosphorus  
oxide,<sup>21,22</sup> and carbon.<sup>23</sup> The filled amorphous glass phases  
provide structural support, and inhibit the growth of nano-  
crystals during the high-temperature treatment, thus reinforcing  
10 the mesoporous frameworks. This has resulted in TiO<sub>2</sub> and  
Nb<sub>2</sub>O<sub>5</sub> with highly crystalline frameworks to date.<sup>23</sup>

Herein we describe the first direct low-temperature, liquid  
crystal surfactant template–crystallization route from aqueous  
solution to form a quasi-ordered crystalline mesoporous  
RuO<sub>2</sub>·0.4H<sub>2</sub>O. The high fundamental specific capacitance of  
15 RuO<sub>2</sub>, along with long cycle life, electrical conductivity, excellent  
charge/discharge rates, and good reversibility<sup>13–15</sup> has inspired  
much effort to elaborate its morphology. Supporting RuO<sub>2</sub> on  
carbon greatly increases the available surface area, for example,  
but at the expense of greatly reducing the density. Our method  
20 constitutes a novel direct approach to the crystalline oxide, which  
is constructed of nanosized metal oxide building blocks on the  
order of several nano-metres in size that are assembled into thin  
walls. In this approach, cationic surfactants serve as pore-  
directing agents instead of non-ionic surfactants or inverse  
25 templates as previously reported. We selected hexadecyl-trimethyl-  
ammonium chloride, C<sub>16</sub>TMA<sup>+</sup>Cl<sup>-</sup>, which can participate in  
an indirect S<sup>+</sup>X<sup>-</sup>I<sup>+</sup> interaction<sup>2</sup> mediated by the chloride ion, and  
thus coordinate a cationic ruthenium nitrosyl precursor. Gentle  
decomposition of the initially formed mesostructured metal  
30 cation–surfactant composite leads to crystallization of the wall  
structure as NO is released. The metal cations are cross-linked to  
form M–O–M bonds, and transformed into the nanosized  
RuO<sub>2</sub>·xH<sub>2</sub>O building blocks. The slow oxidative hydrolysis and  
condensation of the ruthenium oxide precursor are critical to the  
35 low-temperature crystallization process necessary to the  
synthesis. The nanocrystals further form three-dimensional  
networks during calcination to remove the surfactant. The  
promising electrochemical properties of our porous RuO<sub>2</sub>·xH<sub>2</sub>O  
result from a more highly ordered structure and almost tripled  
40 surface area (190 m<sup>2</sup> g<sup>-1</sup>) compared to that obtained from the  
nanocasting method.<sup>10</sup> Crystalline mesoporous RuO<sub>2</sub>·0.4H<sub>2</sub>O  
exhibits a high capacitance of 410 F g<sup>-1</sup> and good rate capability,  
and the amorphous mesoporous RuO<sub>2</sub>·1.3H<sub>2</sub>O reported here  
displays capacitance of over 700 F g<sup>-1</sup>. In view of the wide  
45 applications of RuO<sub>2</sub> as described above, these new materials  
may also open up other avenues of research.

## Materials and characterization

### Synthesis of materials

To prepare templated mesostructured RuO<sub>2</sub>, **1**, 0.8 g of 25% (w/  
w) aqueous hexadecyl-trimethylammonium chloride (Fluka)  
solution, 6.6 g of ruthenium(III) nitrosyl nitrate solution (1.53  
55 wt% Ru, Sigma-Aldrich), and 2.0 g of deionized water were  
mixed in a 20 mL glass bottle and stirred for 1 h at room  
temperature. The solution was transferred to a 100 °C oven and  
heated for 12 h with the bottle tightly capped. Subsequently, 2.0 g  
of a 2 M aqueous NaOH solution were added; and the solution

was vigorously stirred for 6 h at room temperature, transferred to  
1 the 100 °C oven and heated for another 12 h. The reaction  
mixture was filtered and washed with copious amounts of  
deionized water and dried in air at 60 °C to yield **1** (typically 0.2  
5 g). For the synthesis of mesoporous **3**, **1** was heated in a forced  
convection oven for more than 36 h at 200 °C. Less than 36 h  
heating resulted in the hydrous amorphous phase, **2**. Meso-  
porous, crystalline rutile (coherence length of 5.3 nm) RuO<sub>2</sub>, **4**,  
was obtained by heating **1** in 48 h at 200 °C.

### Characterization

Powder X-ray diffraction was performed using a Bruker D8-  
Advance powder diffractometer using Cu-K<sub>α1</sub> radiation (λ =  
1.5405 Å). Scanning electron microscopy (SEM) samples were  
15 sputter coated with gold and imaged using a LEO 1530 field-  
emission SEM equipped with an EDX attachment (Zeiss).  
Images were recorded using a 10 kV accelerating voltage with  
a secondary electron detector. Transmission electron microscopy  
(TEM) was carried out on a Hitachi HD-2000 operating at 200  
20 keV. TGA was performed using a TA Instruments SDT Q600  
system with air as the carrier gas (100 cc min<sup>-1</sup>) and a heating rate  
of 5 °C min<sup>-1</sup>.

Nitrogen adsorption and desorption isotherms were measured  
at 77 K using a Quantachrome AUTOSORB-1 system. Samples  
25 were outgassed at 150 °C under vacuum line for at least 12 h  
before each measurement. The Brunauer–Emmett–Teller (BET)  
method was utilized to calculate the surface area by taking at  
least three data points  $P/P_0 < 0.3$ . Pore size distributions were  
calculated using the Barrett–Joyner–Halenda (BJH) method  
30 applied to the desorption branch of the isotherm.

FTIR spectra were measured using a Bruker Vertex 70 FT-IR  
spectrometer in the spectral range from 1000 to 4000 cm<sup>-1</sup>.

### Electrochemistry

For capacitance measurements, the cyclic voltammetric behavior  
between 0 and 0.9 V (vs. Ag/AgCl) was examined in a three-  
electrode electrochemical cell in a 0.5 M H<sub>2</sub>SO<sub>4</sub> aqueous solu-  
40 tion, using platinum wire as the working electrode and Ag/AgCl  
as the reference electrode. The working electrode was fabricated  
by mixing as-synthesized RuO<sub>2</sub> powder with 3% polyvinylidene  
fluoride (PVdF) binder and casting the mixture on a stainless  
steel current collector. The typical loading of active material was  
approximately 2 mg cm<sup>-2</sup>, and the electrode area was 0.6 cm<sup>2</sup>.  
45 The lithium insertion properties were measured by assembling  
Swagelok-type cells that were galvanostatically discharged at  
a rate of 10 mA g<sup>-1</sup> from their initial open circuit voltage to 1.5 V.  
For cathode fabrication, powders were mixed with 16% Super S  
and 4% polytetrafluoroethylene (PTFE) as a binder, coated onto  
aluminium foil, and dried in a vacuum oven at 80 °C overnight.  
50 The cells were assembled in an argon glove box using lithium  
metal as the anode, glass wool as a separator and 1 M LiPF<sub>6</sub> in 1 :  
1 ethylene carbonate/dimethyl carbonate co-solvent as the elec-  
trolyte.

## Results and discussion

The porous samples were prepared starting from surfactant-  
templated RuO<sub>2</sub> (**1**), followed by gradual removal of the

surfactant by subsequent heat-treatment. The low-angle powder X-ray diffraction (XRD) patterns for the surfactant-templated ruthenium nano-composite (**1**), the amorphous mesoporous RuO<sub>2</sub> formed following template removal (**2**), and the crystalline mesoporous RuO<sub>2</sub> formed after annealing (**3**) are shown in Fig. 1a. For **1**, the reflection at 1.86° was indexed as (100) and indicates the formation of a mesostructure having an inter-planar *d* spacing of 4.7 nm, as expected for a hexagonal mesostructure templated by C<sub>16</sub>TMA<sup>+</sup>Cl<sup>-</sup>.<sup>2</sup> Gentle calcination of **1** for 12 h at 200 °C to remove the surfactant results in the formation of amorphous mesoporous RuO<sub>2</sub> (**2**), as shown in the wide-angle XRD pattern in Fig. 1b. More prolonged heating (12–36 h at 200 °C) nucleates the growth of nanocrystallites of RuO<sub>2</sub> within the wall structure, a process that is controlled by kinetics. The wide-angle diffraction pattern initially shows poorly resolved reflections corresponding to the rutile phase of RuO<sub>2</sub>, which sharpen upon further heat treatment (Fig. 1b). The broadness of the reflections, as estimated by application of the Scherrer equation, suggests a coherence length of about 5.3 nm for the more crystalline, but still porous sample (**4**). The crystallite size of the initial poorly crystalline sample (**3**) is considered to be on the order of the wall thickness of the mesoporous material, about 1.5 nm. The low-angle reflections of **2** and **3** have reduced intensities and are broader than those of **1**, suggesting slight disordering of the mesostructure during heating. The shift of the main reflection to higher angle for the mesoporous products is consistent with a contraction of the pores upon removal of the surfactant, to give an inter-planar *d* spacing of approximately 3.5 nm. The water

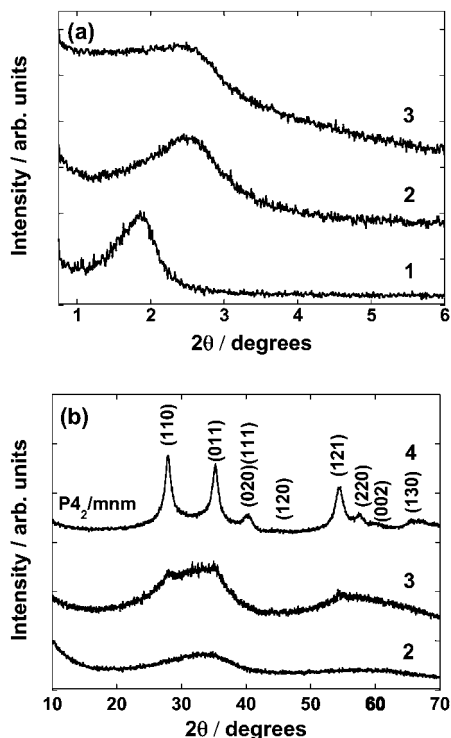


**Fig. 1** (a) Low-angle and (b) wide-angle powder XRD patterns of mesostructured and mesoporous RuO<sub>2</sub>. The symbol 1 represents surfactant-templated mesostructured Ru compound, whereas 2, 3, and 4 refer to RuO<sub>2</sub> from **1** heat-treated at 200 °C for 12 h, 36 h, 48 h respectively.

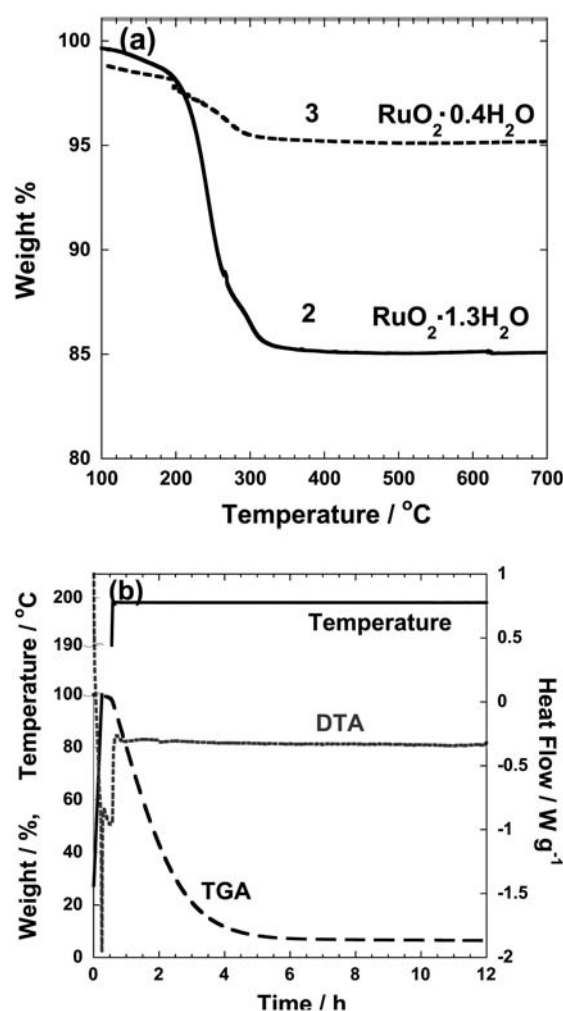


**Fig. 2** (a) Thermogravimetric analysis for amorphous and crystalline mesoporous RuO<sub>2</sub>. The water content *x* in RuO<sub>2</sub>·*x*H<sub>2</sub>O was determined by the ratio of initial and final weight of the sample. (b) TGA/DTA of the pure surfactant on isothermal annealing at 200 °C. The temperature was raised to 200 °C using a 10 °C min<sup>-1</sup> rate, and decomposition was complete after 6 h at 200 °C.

content of **2** and **3** was evaluated by thermogravimetric analysis (TGA) in Fig. 2a. The residual mass at 700 °C was compared with that at 200 °C to determine the water content in the crystalline structure, RuO<sub>2</sub>·*x*H<sub>2</sub>O. The carbon residue in the sample from the decomposition of organic compounds based on chemical analysis is almost negligible (0.2%, see Experimental). TGA analysis of the pure surfactant also showed only a relatively low (6%) residue after a temperature hold at 200 °C for 12 h (Fig. 2b). For the amorphous sample **2** heated for 2 h at 200 °C, the material contains 1.3 water molecules per RuO<sub>2</sub>, considered to be ideal for pseudocapacitor properties.<sup>13–15</sup> The stoichiometry of the crystalline material obtained on more prolonged heating (36 h at 200 °C) was estimated to be RuO<sub>2</sub>·0.4H<sub>2</sub>O. Removal of the water of hydration occurs simultaneously with structural crystallization.

The nanosized character of the mesostructured materials is shown in the SEM images in Fig. 3, which reveal the plate-shaped primary particles of **1** to have basal dimensions of about 100 nm.

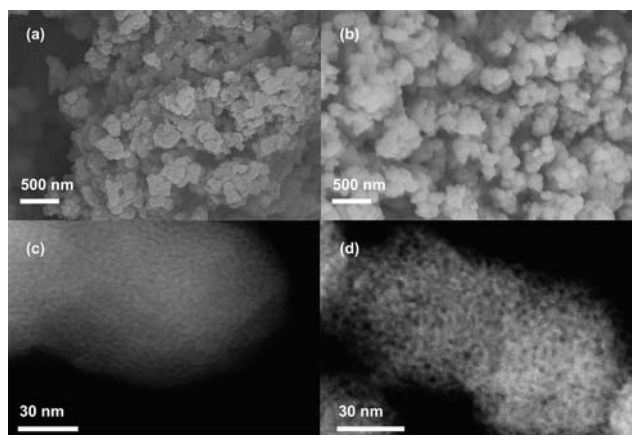


**Fig. 3** SEM (upper) and TEM (lower) images of templated mesostructured RuO<sub>2</sub> (**1**) (a, c); and quasi-ordered crystalline mesoporous RuO<sub>2</sub> (**3**), (b, d).

The overall morphologies before and after surfactant removal and crystallization of the RuO<sub>2</sub> wall structure, *i.e.*, of **1** and **3** were very similar. This is best demonstrated by the high resolution TEM images. The surfactant-laden mesostructured RuO<sub>2</sub>, **1**, shows a relatively smooth surface structure with an underlying “worm-like” pattern, reminiscent of mesoporous silica produced from non-ionic surfactant templating routes.<sup>24</sup> The single peak in the XRD low-angle pattern arises from the regular pore size and wall thickness throughout the overall structure. The partially crystallized RuO<sub>2</sub>, **3**, displays the same particle morphology, but the porous structure of the framework created by the removal of the surfactant is clearly visible. Homogeneously sized mesopores about 2 nm in diameter are evident. The overall morphology and order are similar to those of crystalline TiO<sub>2</sub> obtained by polymer-mediated “scaffold” templating,<sup>23</sup> but the pore dimensions and wall thickness are smaller by almost an order of magnitude, and the surface area is much higher. This accounts for the much higher surface area of our material, which is necessary for good catalytic and/or capacitance properties.

Nitrogen adsorption measurements on **3** at 77 K (Fig. 4b) reveal a very high surface area and pore volume, of 190 m<sup>2</sup> g<sup>-1</sup> and 0.12 cm<sup>3</sup> g<sup>-1</sup>, respectively (the BET plot is depicted in Fig. 4c). Normalized to mesoporous carbon, this surface area/pore volume corresponds to a respectable 2162 m<sup>2</sup> g<sup>-1</sup> and 1.37 cm<sup>3</sup> g<sup>-1</sup>. It is higher than the values obtained for mesoporous crystalline Nb<sub>2</sub>O<sub>5</sub>, of 72 m<sup>2</sup> g<sup>-1</sup>, although that material exhibited much larger mesopores (20 nm).<sup>23</sup> The pore size distribution was calculated by applying the Barrett–Joyner–Halenda algorithm to the desorption branch data. A minor portion of mesopores around 4 nm and 6 nm is present, in addition to a large proportion of micropores and mesopores centered around 2 nm. The latter represent the main structural porosity as indicated in the TEM image in Fig. 3d. The high surface area of this material is created by these small-sized and multiple pore structures. This variation is ideal for supercapacitor properties.<sup>25,26</sup> The amorphous porous material **2** possesses a substantially larger surface area of more than 260 m<sup>2</sup> g<sup>-1</sup>. However, about a third of the pore volume is contributed by the micropores as measured by the *t*-plot analysis (Fig. 4d) and summarized in Table 1. These

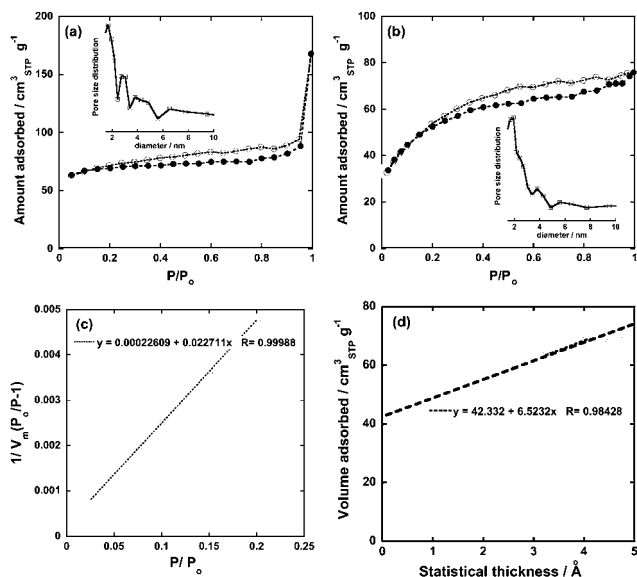


**Fig. 4** Nitrogen sorption isotherms measured at 77 K and corresponding BJH pore size distributions (inset) (a) for amorphous mesoporous RuO<sub>2</sub> (**2**) and (b) for quasi-ordered crystalline mesoporous RuO<sub>2</sub> (**3**). BET plot for crystalline mesoporous RuO<sub>2</sub> (c); and *t*-plot for amorphous RuO<sub>2</sub> (d). The micropore volume was calculated from the *y*-intercept of the graph.

**Table 1** Physical properties of mesoporous ruthenium precipitate, amorphous RuO<sub>2</sub>·1.3H<sub>2</sub>O, and crystalline mesoporous RuO<sub>2</sub>·0.4H<sub>2</sub>O

Material	$d_{(100)}/\text{nm}$	Surface area/m <sup>2</sup> g <sup>-1</sup>	Pore volume/cm <sup>3</sup> g <sup>-1</sup>	Micropore volume/cm <sup>3</sup> g <sup>-1</sup>
<b>1</b>	4.7	—	—	—
<b>2</b>	3.5	263	0.20	0.07
<b>3</b>	3.5	190	0.12	0

micropores collapse as crystallization proceeds. The origin of the microporosity in the amorphous material can be addressed by consideration of the chemistry used to assemble the mesostructure.

The common self-assembly mechanisms invoked when cationic surfactants are used include direct S<sup>+</sup>I<sup>-</sup> or indirect S<sup>+</sup>X<sup>-</sup>I<sup>+</sup> pathways.<sup>2</sup> The direct S<sup>+</sup>I<sup>-</sup> pathway involves the co-condensation of anionic inorganic species with a cationic surfactant, as in the synthesis of MCM-41.<sup>1</sup> In the indirect S<sup>+</sup>X<sup>-</sup>I<sup>+</sup> pathway, the organic–inorganic self-assembly is mediated by negatively charged ions (usually chloride or bromide).<sup>2</sup> In the present case, the chemical analysis for the initial surfactant-laden ruthenium mesostructure (**1**) measured by energy dispersive X-ray (EDX) spectroscopy indicates a chloride/C<sub>16</sub>TMA<sup>+</sup> ratio close to 1. The FTIR spectrum of **1** shown in Fig. 5a also reveals the presence of nitrosyl and hydroxyl species. The TGA of **1** using isothermal annealing at 200 °C (Fig. 5b) shows that decomposition to RuO<sub>2</sub> (59 wt%) occurs after 12 h. Hence we propose that the inorganic–organic self-assembly is synthesized through an indirect S<sup>+</sup>X<sup>-</sup>I<sup>+</sup> pathway mediated by the chloride ion expressed as C<sub>16</sub>TMA<sup>+</sup><Cl<sup>-</sup>>Ru(NO)(OH)<sub>x</sub>(H<sub>2</sub>O)<sub>y</sub>. The slow decomposition and release of nitric oxide are the source of micropores in the amorphous material. It is reported that MCM-

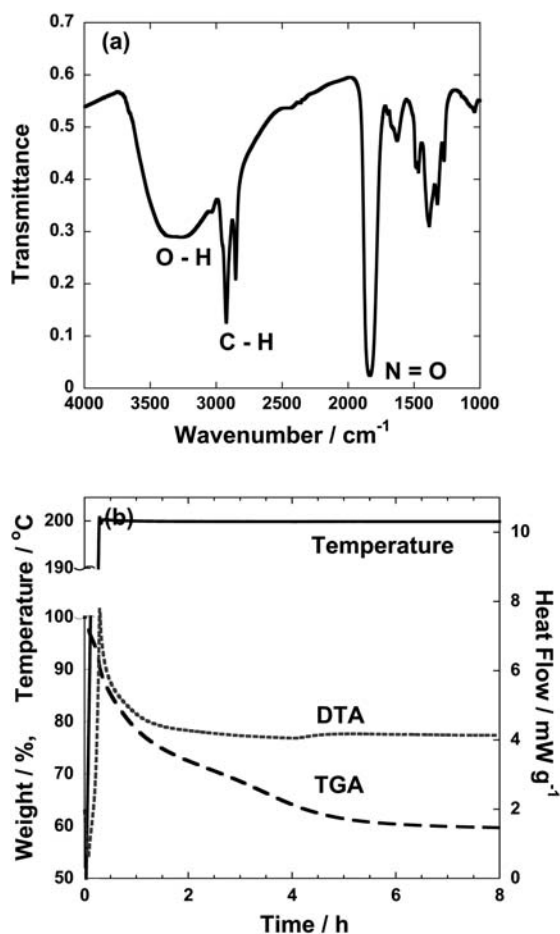


**Fig. 5** (a) FTIR spectrum of **1** showing the presence of hydroxyl and nitrosyl functional groups. The absorption at 1836 cm<sup>-1</sup> is red-shifted compared to gaseous nitric oxide (1876 cm<sup>-1</sup>),<sup>27</sup> ascribed to complexation of the mononitrosyl species to Ru(III). (b) TGA/DTA profiles of the ruthenium precipitate on isothermal annealing at 200 °C. The temperature was raised to 200 °C using a 10 °C min<sup>-1</sup> rate. Decomposition was complete after 6 h at 200 °C.

41 formed in alkaline solution synthesized by a direct S-I<sup>+</sup> pathway has no significant chloride content using a similar surfactant, for example.<sup>2</sup> The high surface area and interconnected small-mesopore network based on RuO<sub>2</sub>·xH<sub>2</sub>O nanocrystallites suggest these materials should behave as promising supercapacitors. To investigate their properties, the materials were cast from slurries as “thick” conventional electrodes onto stainless steel current collectors, and electrochemically cycled in 0.5 M H<sub>2</sub>SO<sub>4</sub> in the voltage range 0–0.9 V, at a scan rate between 2 and 200 mV s<sup>-1</sup>. Cyclic voltammetry experiments conducted on the amorphous RuO<sub>2</sub>·1.3H<sub>2</sub>O (**2**) mesoporous electrodes heat-treated at 200 °C for 12 h exhibited a high capacitance of 700 F g<sup>-1</sup>, comparable to that of other hydrous amorphous ruthenium oxides that range from 600–900 F g<sup>-1</sup>.<sup>28</sup> However, some irreversibility at low potential (Fig. 6a) and poor retention of capacitance with increasing sweep rate (200 F g<sup>-1</sup> at 20 mV s<sup>-1</sup>) were observed, characteristic of amorphous hydrous RuO<sub>2</sub>.<sup>28</sup> Whereas the capacitive response benefits from the hydrous content that enables proton transfer, the poor electronic conductivity of the amorphous framework impedes electron

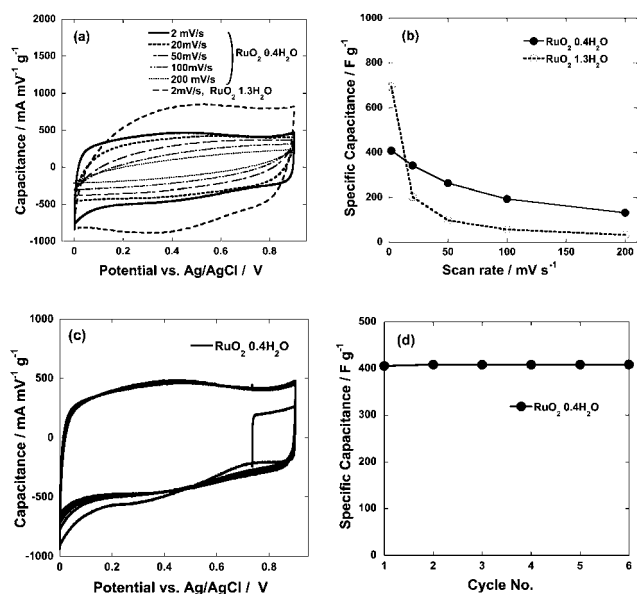


**Fig. 6** (a) Cyclic voltammograms and (b) average specific capacitance obtained for mesoporous crystalline RuO<sub>2</sub>·0.4H<sub>2</sub>O (**3**) or amorphous RuO<sub>2</sub>·1.3H<sub>2</sub>O (**2**) at different scan rates in 0.5 M sulfuric acid; (c, d) capacitance of RuO<sub>2</sub>·0.4H<sub>2</sub>O on cycling.

transport. The response of the capacitance vs. potential curves of the crystalline RuO<sub>2</sub>·0.4H<sub>2</sub>O, however, displays a close-to-ideal rectangular shape and perfect electrochemical reversibility of the redox reactions. The capacitance of 410 F g<sup>-1</sup> at 2 mV s<sup>-1</sup> was only slightly lowered to 400 F g<sup>-1</sup> on increasing the sweep rate to 20 mV s<sup>-1</sup>. Fig. 6b shows the variation of specific capacitance with scan rate, indicating very good retention. High capacitance (up to 1000 F g<sup>-1</sup>) has recently been reported for RuO<sub>2</sub>·xH<sub>2</sub>O films (55 nm in thickness) with a very large pore dimension of 15–30 nm prepared by an evaporation self-assembly (EISA) technique, but comparison is difficult owing to the ultra-thin (55 nm) nature of these films.<sup>29</sup> The capacitance value we report here measures up reasonably well, taking into account the fact that our materials properties are reported for bulk cast electrodes, and that electronic contact to the current collector and transport are enhanced by up to a factor of 5–10 for thin membranes. The values we report are comparable or superior to other “bulk” cast crystalline RuO<sub>2</sub>·xH<sub>2</sub>O materials at similar sweep rates (*e.g.* 75 F g<sup>-1</sup> at 20 mV s<sup>-1</sup> V;<sup>13</sup> and 350 F g<sup>-1</sup> at 2 mV s<sup>-1</sup> V).<sup>30</sup>

This performance can be attributed to the 3-D interconnected network of pores and framework, which facilitates ion and electron transport. The mesoporous network of RuO<sub>2</sub>·xH<sub>2</sub>O also reduces the resistance to electrolyte penetration, and the nanoscopic RuO<sub>2</sub>·xH<sub>2</sub>O crystallites promote rapid proton exchange, and electron transfer.

The large surface area and nano-scale wall thickness as well as electrolyte accessibility through the nano-channels of the mesoporous RuO<sub>2</sub> can also influence its lithium insertion properties dramatically due to the enhanced kinetics implemented by the shorter diffusion path.<sup>31,32</sup> In the present case, as shown in Fig. 7a and b, the intercalation of lithium into the mesoporous material shows drastically different behavior compared to that of the bulk. By downsizing the crystallite size to the nano-metre scale,

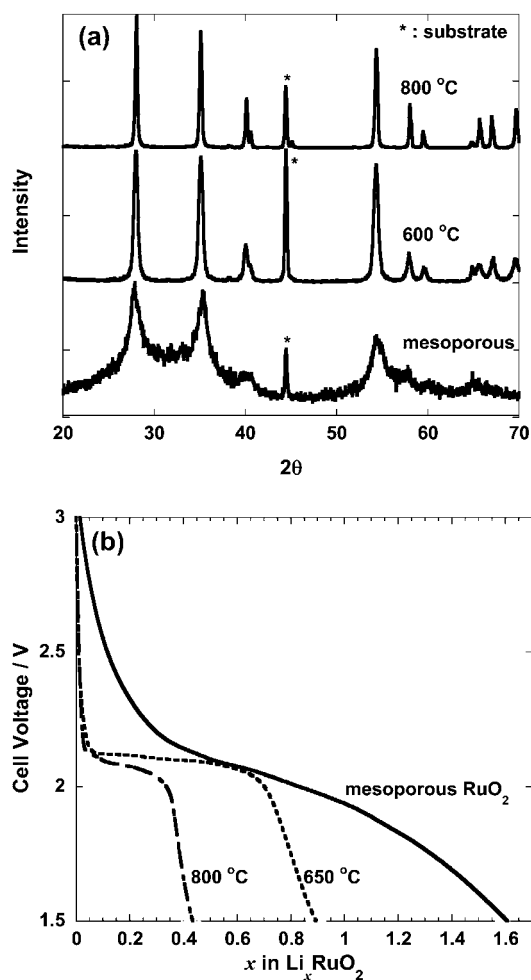


**Fig. 7** (a) Powder X-ray diffraction patterns for mesoporous RuO<sub>2</sub> (4); after heating at 600 °C (crystallite size = 17 nm) and at 800 °C (crystallite size = 30 nm). (b) Electrochemical discharge profiles of the intercalation of Li<sup>+</sup>/e<sup>-</sup> in ruthenium oxide for the samples heat-treated at the temperatures indicated. As the crystallite size decreases, the electrochemical activity of the material greatly increases. Crystallite sizes were calculated from the Scherrer equation,  $c = 0.9\lambda/B \cos \theta$ , where  $B$  represents the full width of the half maximum of the (110) reflection in the corresponding XRD pattern.

the redox accessibility of ruthenium dioxide is greatly increased, and much higher discharge capacity for the material with the mesoporous morphology is observed. The sloping potential of this material (in contrast to the plateau characteristic of the bulk) also implies a change in the lithium insertion reaction mechanism, which is beneficial in terms of Li<sup>+</sup> ion diffusion in the solid.<sup>31</sup>

## Conclusions

In conclusion, a facile synthetic route to quasi-ordered crystalline mesoporous RuO<sub>2</sub> oxide has been developed by a cationic surfactant template route that follows an indirect S<sup>+</sup>X<sup>-</sup>I<sup>+</sup> pathway. The initially templated amorphous hydrated RuO<sub>2</sub> was converted to a framework containing nanocrystallite surface-hydrated RuO<sub>2</sub> after surfactant removal by slow annealing, to

form a pore structure exhibiting multiple mesoporosity. The high surface area, large pore volume and nanosized wall structure of this mesoporous material result in good properties as an electrode material for energy storage devices, especially supercapacitors. The material also has potential as a catalyst for chemical reactions, as will be reported subsequently.

## Notes and references

- C. T. Kresge, M. E. Leonowicz, W. J. Roth, J. C. Vartuli and J. S. Beck, *Nature*, 1992, **359**, 710.
- Q. Huo, D. I. Margolese, U. Ciesla, P. Feng, T. E. Gier, P. Sieger, R. Leon, P. M. Petroff, F. Schüth and G. D. Stucky, *Nature*, 1994, **368**, 317.
- H. Shibata, T. Ogura, T. Mukai, T. Ohkubo, H. Sakai and M. Abe, *J. Am. Chem. Soc.*, 2005, **127**, 16396.
- J. Deng, L. Zhang, H. Dai and C.-T. Au, *Appl. Catal., A*, 2009, **352**, 43.
- J.-Y. Luo, Y.-G. Wang, H.-M. Xiong and Y.-Y. Xia, *Chem. Mater.*, 2007, **19**, 4791.
- D. Wang, D. Choi, Z. Yang, V. V. Viswanathan, Z. Nie, C. Wang, Y. Song, J.-G. Zhang and J. Liu, *Chem. Mater.*, 2008, **20**, 3435.
- Y.-S. Hu, Y.-G. Guo, W. Sigle, S. Hore, P. Balaya and J. Maier, *Nat. Mater.*, 2006, **5**, 713.
- X. Cui, Q. He, F. Cui, J. Zhao, L. Li, H. Chen and J. Shi, *Dalton Trans.*, 2009, 3395.
- L. Wang, D. Li, R. Wang, Y. He, Q. Qi, Y. Wang and T. Zhang, *Sens. Actuators, B*, 2008, **133**, 622.
- W. Shen, J. Shi, H. Chen, J. Gu, Y. Zhu and X. Dong, *Chem. Lett.*, 2005, **34**, 390.
- O. Delmer, P. Balaya, L. Kienle and J. Maier, *Adv. Mater.*, 2008, **20**, 501.
- D. W. Murphy, F. J. Di Salvo, J. N. Carides and J. V. Waszczak, *Mater. Res. Bull.*, 1978, **13**, 1395.
- I. H. Kim and K. B. Kim, *J. Electrochem. Soc.*, 2006, **153**, A383.
- J. P. Zheng and T. R. Jow, *J. Electrochem. Soc.*, 1995, **142**, L6.
- I. H. Kim and K. B. Kim, *J. Electrochem. Soc.*, 2004, **157**, E7.
- F. Jiao, A. Harrison, J. Jumas, A. V. Chadwick, W. Kockelmann and P. G. Bruce, *J. Am. Chem. Soc.*, 2006, **128**, 5468.
- F. Jiao and P. G. Bruce, *Adv. Mater.*, 2007, **19**, 657.
- K. M. Shaju, F. Jiao, A. Débart and P. G. Bruce, *Phys. Chem. Chem. Phys.*, 2007, **9**, 1837.
- F. Jiao, A. H. Hill, A. Harrison, A. Berko, A. V. Chadwick and P. G. Bruce, *J. Am. Chem. Soc.*, 2008, **130**, 5262.
- X. Lai, X. Li, W. Geng, J. Tu, J. Li and S. Qiu, *Angew. Chem., Int. Ed.*, 2007, **46**, 738.
- H.-S. Yun, H. Zhou and I. Honma, *Chem. Commun.*, 2004, 2836.
- D. Li, H. Zhou and I. Honma, *Nat. Mater.*, 2004, **3**, 65.
- J. Lee, M. C. Orilall, S. C. Warren, M. Kamperman, F. J. Disalvo and U. Wiesner, *Nat. Mater.*, 2008, **7**, 222.
- P. Simon and Y. Gogotsi, *Nat. Mater.*, 2008, **7**, 845.
- S.-S. Kim, T. R. Pauly and T. J. Pinnavaia, *Chem. Commun.*, 2000, 835.
- I. Park and T. J. Pinnavaia, *Microporous Mesoporous Mater.*, 2009, **118**, 239.
- C. Drouet, P. Alphonse and A. Rousset, *Phys. Chem. Chem. Phys.*, 2001, **3**, 3826.
- J. P. Zheng, P. J. Cygan and T. R. Jow, *J. Electrochem. Soc.*, 1995, **142**, 2699; W. Lee, R. S. Man, V. V. Todkar, S. Lee, O. Egorava, W.-S. Chae and S.-H. Han, *Electrochem. Solid-State Lett.*, 2007, **10**, A225; J. Long, K. Swider, C. Merzbacher and D. Rolison, *Langmuir*, 1999, **15**, 780.
- C. Sassoie, C. Laberty, H. L. Khanh, S. Cassaignon, C. Boissiere, M. Antonietti and C. Sanchez, *Adv. Funct. Mater.*, 2009, **19**, 1922.
- Y.-S. Hu, Y.-G. Guo, W. Sigle, S. Hore, P. Balaya and J. Maier, *Nat. Mater.*, 2006, **5**, 713.
- M. Wagemaker, W. J. H. Borghols and F. M. Mulder, *J. Am. Chem. Soc.*, 2007, **129**, 4323.
- M. Okubo, E. Hosono, J. Kim, M. Enomoto, N. Kojima, T. Kudo, H. Zhou and I. Honma, *J. Am. Chem. Soc.*, 2007, **129**, 7444.

# 1 Authors Queries 1

Journal: JM

5 Paper: b926734d 5

Title: Direct synthesis of electroactive mesoporous hydrous crystalline RuO<sub>2</sub> templated by a cationic surfactant

Editor's queries are marked like this... **1**, and for your convenience line numbers are inserted like this... 5

Query Reference	Query	Remarks
15 1	For your information: You can cite this article before you receive notification of the page numbers by using the following format: (authors), J. Mater. Chem., (year), DOI: 10.1039/ b926734d.	
20 2	Please check that the TOC text fits within the allocated space indicated on the front page of the proof. If the entry does not fit between the two horizontal lines, then please trim the text and/or the title.	